2023

Assessing the utility of 3D modeling with photogrammetry in assigned sex estimation from the greater sciatic notch

BOSTON UNIVERSITY

ARAM V. CHOBANIAN & EDWARD AVEDISIAN SCHOOL OF MEDICINE

Thesis

ASSESSING THE UTILITY OF 3D MODELING WITH PHOTOGRAMMETRY IN ASSIGNED SEX ESTIMATION FROM THE GREATER SCIATIC NOTCH

by

CHELSEA MADISON CARRIÈRE

B.S., Rutgers, The State University of New Jersey, 2020

Submitted in partial fulfillment of the

requirements for the degree of

Master of Science

2023

Approved by

First Reader

Sean Tallman, Ph.D.
Assistant Professor of Anatomy and Neurobiology

Second Reader

Tara Moore, Ph.D.
Associate Professor of Anatomy and Neurobiology

ACKNOWLEDGMENTS

I would like to acknowledge the contributions of Dr. Sean D. Tallman and Dr. Tara L. Moore to the completion of this manuscript. Special thanks go to Lance D. Carrière of Vision Driven Solutions and Sam De Lara who were instrumental in the creation of the python-based plug-ins for the programs utilized in this study; without them, this project would not have been possible.

ASSESSING THE UTILITY OF 3D MODELING

WITH PHOTOGRAMMETRY IN ASSIGNED SEX ESTIMATION

FROM THE GREATER SCIATIC NOTCH

CHELSEA MADISON CARRIÈRE

ABSTRACT

Assigned sex estimation via the greater sciatic notch (GSN) is traditionally performed via physical/visual examination and ordinal scoring; however, this relies on the subjective assessment of morphology for typological classification which may not be reflective of human variation. Three-dimensional (3D) photogrammetry may offer a technologically advanced, low cost, and more objective alternative to assess the complex curvature of anatomical landmarks. This research explores the accuracy of photogrammetry derived 3D models by comparing digital measurements to those obtained from the skeletal elements and to streamline the application of curvature analysis for the estimation of assigned sex from the GSN. This study utilizes the left and right os coxae from 15 skeletal individuals (5 females, 10 males) from the Boston University Chobanian & Avedisian School of Medicine. A Fujifilm X-Pro2 and Fujifilm 35 mm prime lens captured 123 images per element, which were processed in Meshroom by AliceVision® to create a 3D textured mesh. The mesh was exported into Blender for cleanup, scaling, measurement, and curvature analysis. The measurements were between 96.54% and 99.94% consistent across methods and observations. The consistency between digital metric observations increased by an average of 0.07% when compared to the consistency of the dry bone measurements. Additionally, curvature analysis of the

GSN correctly estimated the assigned sex of all os coxae in the sample. This study demonstrates that photogrammetry is an accurate and reliable method for the digitization of remains that enables analytical techniques to better capture skeletal variation compared to traditional methods.

TABLE OF CONTENTS

ACKNOWLEDGMENTS iv

ABSTRACT v

TABLE OF CONTENTS vii

LIST OF TABLES ix

LIST OF FIGURES x

LIST OF ABBREVIATIONS xi

GLOSSARY xii

INTRODUCTION 1

The Greater Sciatic Notch in the Estimation of Assigned Sex 1

The Use of 3D Modeling in Forensic and Archaeological Contexts 5

Software 8

MATERIALS AND METHODS 11

Photogrammetry 11

Model Scaling 15

Assigned Sex Estimation 17

RESULTS 21

Evaluation of Reproducibility of Reconstructed 3D Models 21

Evaluation of Biological Sex Estimation from the GSN 24

DISCUSSION 27

Successes and Limitations 27

Future Directions 32

Ethical Considerations 35
CONCLUSION 39
APPENDIX A 41
APPENDIX B 42
APPENDIX C 46
BIBLIOGRAPHY 47
CURRICULUM VITAE 56

LIST OF TABLES

Table 1. Comparison of system specifications utilized throughout data processing. 14

Table 2. R^2 results for dry bone and digital measurement comparisons..... 22

Table 3. Average percent error rates for dry bone and digital measurement comparisons. 22

Table 4. Radii; curvature quotients using the first and second sets of digital measurements; metric sex estimation following Biwasaka et al. (2012); estimated sex following Walker (2005); and known sex for the study sample. Metric sex estimation was established using a cutoff curvature quotient of 7.6 for a spline curve of 60 mm following Biwasaka et al. (2012). Curvature quotients above the cutoff were estimated as female and below the cutoff as male. 26

LIST OF FIGURES

Figure 1. Photo capture setup (left) and BU40-L (right) with scale and wooden supports. 13

Figure 2. Orientation of the GSN of Individual BU35-L in an orthographic view such that the PIIS, DP, and IS are featured in the same plane. 15

Figure 3. Use of the measure tool to adjust the global unit scale with Individual BU35-L. 16

Figure 4. Digital measurements of the OCH, SIB, AH, OFH, and OFB of Individual BU35-L. 17

Figure 5. Mesh of the Bezier curve (orange line) of Individual BU35-L and number of vertices (bottom right red arrow). 18

Figure 6. Best fit circles of Individual BU35-L (left) and Individual BU38-L (right). 19

Figure 7. Comparison of digital measurements 1 and 2. 23

Figure 8. Comparison of dry measurements 2 and digital measurements 1. 23

Figure 9. Textured mesh of BU35-L from the acetabular (left), lateral (middle), and medial (right) views. 28

LIST OF ABBREVIATIONS

2D.....Two dimensional

3D.....Three dimensional

AI ..... Artificial intelligence

BU ..... Boston University

CPU..... Central processing unit

CT .....Computed tomography

CUDA ..... Compute Unified Device Architecture

CQ.....Curvature Quotient

DP .....Deepest Point of the greater sciatic notch

DSLR .....Digital Single-lens Reflex

FSTT .....Facial soft tissue thickness

GPU.....Graphics processing unit

GSN..... Greater sciatic notch

IS .....Ischial Spine

PIIS .....Posterior Inferior Iliac Spine

SfM ..... Structure from Motion

SGM.....Semi-Global Matching

SIFT .....Scale-invariant feature transform

UV.....“U” axis and “V” axis

ZNCC.....Zero mean normalized Cross correlation

GLOSSARY

Bezier curve - a parametric curve used in computer graphics and related fields, usually defined by a single particular polynomial

Biological Profile - consists of estimates of sex, age, ancestry, and stature, built with the intention of aiding in the identification of unidentified human remains

Biological sex - the different biological and physiological characteristics of males and females, such as reproductive organs, chromosomes, hormones, etc; Not an assessment of gender

Curvature quotient - Ratio of the curvature radius to a defined measurement on the same element, e.g. (GSN curvature radius/max os coxa height)*100

Curvature radii - The radius of the best-fit circle or sphere derived from a morphological feature

Edge - The lines where two faces on a 3D shape meet

Face - A flat or curved surface on a 3D shape

Os Coxa(e) - Also known as the innominate bone, pelvic bone, or coxal bone; Formed by the ilium, ischium, and the pubis

Photogrammetry - a three-dimensional coordinate measuring technique that uses photographs as the fundamental medium for metrology or measurement

Polygonal Mesh - a collection of vertices, edges and faces that defines the shape of a polyhedral object

Python - an interpreted, object-oriented, high-level programming language with dynamic semantics developed by Guido van Rossum

Spline curve - a special case of Bezier curve, defined by piecewise polynomials, usually intended to approximate a real-world shape that otherwise has no mathematical representation or whose representation is unknown or too complicated

Texture map - an image applied to the surface of a shape or polygon

Texture Mapping - Process in which a 2D surface is wrapped around a 3D object using vertex coordinate information

UV map/layout - the flat surface representation of a 3D model used to wrap textures

UV mapping - process of projecting a 2D image to a 3D model's surface, the "U" and "V" denote the axes of the 2D texture

Vertex (plural vertices) - a data structure that describes certain attributes, like the position of a point in 2D or 3D space, or multiple points on a surface

INTRODUCTION

The Greater Sciatic Notch in the Estimation of Assigned Sex

An integral part of any forensic anthropological analysis is the building of a biological profile from unidentified human remains, which includes estimations of assigned sex at birth, age at death, stature, and possibly population affiliation. Of these, binarily constructed assigned sex estimation is established first as it informs other parameters of the biological profile. Historically, the pelvis and cranium have been most frequently used for assigned sex estimation (Buikstra & Ubelaker, 1994; Klales et al., 2012; Walker, 2008). The pelvis, especially, is well known to display significant sexual dimorphism in humans due to the functional differences between females and males with regards to parturition. The pubis, in particular, is generally accepted to be one of the best indicators for estimating the sex in adult remains. Studies of the pubis by Phenice (1969) and Klales et al. (2012) demonstrated accurate nonmetric approaches; however, this region may be damaged or missing in forensic and archaeological settings. In incomplete or damaged cases, other features on the ilium can prove useful (Kim et al., 2018), and research has demonstrated that measurements from long bones perform better for sex estimation than the cranium (Patterson & Tallman, 2019; Spradley & Jantz, 2011).

On the ilium, the greater sciatic notch (GSN) is often utilized to aid in the estimation of assigned sex (Buikstra & Ubelaker, 1994; Walker, 2005). The GSN is the notch on the posterior inferior aspect of the ilium, between the posterior inferior iliac spine (superior) and the ischial spine (inferior) where the sciatic nerve travels. This structure, in combination with ligaments, form the greater sciatic foramen through which

the piriformis muscle, superior gluteal nerve, and vascular vessels pass (Kim et al., 2018). Generally, the GSN is wider with a lower width-to-depth ratio in females than in males, which tends to be U-shaped and narrow (Walker, 2005). The GSN is often visually scored on a visual five-point ordinal scale with associated probabilities following Walker (2005): a score of 1 (wide) indicates female, a score of 2 is ambiguous in morphology (sexually indeterminate), scores of 3 and 4 indicate probable male, and a score of 5 (narrow) indicates male. This method was found to be fairly accurate with a success rate of 88% for adult females and a success rate of 91% for adult males in a sample comprised of English individuals from the St. Bride's Collection and African American and European American individuals from the Hamann-Todd Collection (Walker, 2005). Conversely, Buikstra and Ubelaker (1994) offer a five-point ordinal scale without associated probabilities or population scaling. Accordingly, sciatic notch scores of 1 and 2 indicate or suggest female, a score of 3 is ambiguous, and scores of 4 and 5 suggest or indicate male; however, this system was developed for archaeologically derived Native American remains (Buikstra & Ubelaker, 1994). As with adults, the GSN has been found to be a somewhat reliable sex indicator in infant and juvenile skeletal remains (Khomiakov et al., 1987; Nakao, 1998; Schutkowski, 1993; Souri, 1959; Thomson, 1899). Such young individuals tend to be more difficult to identify as most sexually dimorphic traits have not yet developed and are difficult to observe; however, Schutkowski (1993) reported a success rate of 95.0% for males and 71.4% for females when looking at the GSN angle and 81.2% for males and 76.5% for females when observing GSN depth.

Accurate sex estimation from the visual assessment of the GSN following Walker (2005), however, has not been replicated across various populations. Moreover, the reliance on visual assessments of skeletal elements alongside typological diagrams that may not accurately reflect human skeletal variation introduces subjectivity, particularly for morphology that does not fit into the extremes (i.e., scores of 1 and 5). The relatively wide range of "intermediate" values and the inability of the scale to adequately describe the continuous phenotypic variation of the GSN leaves the potential for significant interobserver inconsistencies (Walker, 2005). Forensic anthropologists vary widely in their experience with known-sex collections, and this undoubtedly influences the amount of weight they give to the differences in sciatic notch shape in their sex estimations (Shearer et al., 2012). Gómez-Valdés et al. (2012) tested the accuracy of the ordinal scoring method from Walker (2005) and only achieved a correct classification rate of 68.5% in their sample from a contemporary Mexican population. Many researchers have attempted to eliminate these inconsistencies by developing metric approaches that involve discriminant function analysis, coordinate geometric morphometrics, and probabilistic morphological analysis (Bytheway & Ross, 2010; Gómez-Valdés et al., 2012; Rogers & Saunders, 1994; Steyn & İşcan, 2008). Some approaches attempt to measure the distances between landmarks and the angles of the GSN while others utilize computer aided geometric morphometric methods to quantify the outline of the curve (Gonzalez et al., 2009; Kim et al., 2018). However, these too can introduce intra- and inter-observer error as the measurement process is performed with manually defined

points and handheld instruments such as sliding calipers or protractors from which the resulting measurement values may differ.

To mitigate reliability and methodology issues associated with the pelvis, Biwasaka et al. (2012) used 3D models constructed from computed tomography (CT) scans to apply a novel metric curvature analysis which resulted in a comparative measurement error of 1 - 2 mm and was thus deemed acceptable for anthropological analysis (Biwasaka et al., 2009, 2012). The authors analyzed three areas of curvature within the pelves of contemporary Japanese individuals: the pubic arch, the greater pelvis (the space enclosed by the pelvic girdle above and in front of the pelvic brim, bounded on either side by the ilium), and the GSN (Biwasaka et al., 2012; Clemente, 1985). The researchers contended that 3D curvature analysis allows for the reconstruction of subtle, intuitional morphological differences not clearly captured in 2D methods. For the GSN analysis, the models were taken from a lateral view and a 2D mathematical spline curve was set along the outline of the GSN. Subsets of this curve measuring 5, 10, 20, 30, 40, 50 and 60 mm in length were then used to create a series of best-fit circles. Six coordinate points from each of the subsets were used in the simulated annealing method to compute the circles. The radii of these circles, which the authors refer to as the curvature radii, were then divided by the maximum iliac height to account for variation in pelvic size between individuals. This resulting ratio was then multiplied by 100 to create the curvature quotient. Similar curvature quotients were created using the pelvic arch (*radius / pelvic breadth x 100*) and greater pelvis (*radius / iliac breadth x 100*). In each analysis, the curvature quotient was used to estimate the assigned sex of the individual. In all cases

except for the greater pelvis, the curvature radii and curvature quotients were found to be significantly different between the sexes and appropriate for sex estimation. For the GSN, the best separation of females and males was found at a curve length of 60 mm and a cutoff curvature quotient of 7.6, above which were estimated as female and below which were estimated as male. Sex was correctly estimated in 89.1% of individuals: 93.8% correct in the males and 83.7% correct in the females. For a shorter curve length of 10 mm and a cutoff curvature quotient of 4.1, correct sex estimation from the GSN was reduced to 82.0%: 85.8% for males and 77.6% for females. These novel methods demonstrated significant potential for practical applications in forensic anthropology as curvature analysis can be applied to damaged or incomplete elements and they mitigate the subjectivity associated with ordinal scoring (Biwasaka et al., 2012).

The Use of 3D Modeling in Forensic and Archaeological Contexts

Application of computer software to obtain osteometrics may greatly increase the reproducibility and consistency of the measurements, regardless of operator or observer. Many researchers have experimented with the use of 3D modeling in archaeology and forensic anthropology (Jani et al., 2020; Johnson et al., 2020; Koutsoudis et al., 2013; Peckmann et al., 2015). Using these models, researchers have derived computer assisted measurements using the 3D mesh's coordinate information of each landmark and planes. One of the most detailed ways to create 3D models is with CT scan data, which were found to produce measurements with average error rates of only 1.9% and 0.86% when compared to associated dry bone measurements (Biwasaka et al., 2009). The digital

nature of CT scans also allowed for coordinate and metric information to be easily recorded and stored for later reassessments and validation studies (Kim et al., 2018). However, widespread application of this 3D modeling method is unrealistic in most settings as the machines themselves are expensive, require experienced personnel to operate, and the materials being scanned must be transported to the machine's location (Perrone & Williams, 2019; Weber & Bookstein, 2011). Another promising method of digitization is through a surface laser scanner (Jani et al., 2020; Johnson et al., 2020; Kuzminsky & Gardiner, 2012; Perrone & Williams, 2019). While there are a variety of surface laser scanners available, they are likewise costly and require experienced personnel to operate and are thus unlikely to be put into widespread anthropological use (Kuzminsky & Gardiner, 2012; *NextEngine 3D Laser Scanner*, 2020).

Structure-from-Motion (SfM) photogrammetry poses a possible solution to the difficulties associated with CT and laser scanning. SfM is a 2D to 3D modeling technique that utilizes photographic datasets or photosets to create the digital mesh of an object. This can be achieved with widely available equipment including digital (DSLR or mirrorless) cameras, open-source or commercial processing software, and a standard computer (Church, 2019). The SfM technique is unique in that it is low cost and can be utilized effectively in the lab or field without having to transport cumbersome equipment. Current research has been successful in utilizing this method of photogrammetry in archaeology with reconstructing human skeletal remains and low feature artifacts for public engagement as well as in forensics with crime scene reconstruction (Church, 2019; Koutsoudis et al., 2013; Omari et al., 2020; Redford et al., 2020).

Omari et al. (2020) and Redford et al. (2020) both utilized a SfM method where the camera rotated around a stationary object. Redford et al. (2020) digitally reconstructed a highly fragmented skeleton found in a 13th century mass grave in Sidon, Lebanon. The authors sought to create usable 3D models through a streamlined photogrammetric workflow involving several advanced 3D design commercial softwares. They created their photosets with a Canon EOS 5D Mk. III DSLR camera mounted on a homemade orbiting camera rig. With this rig, the camera was moved around the stationary target object at a consistent angle to capture each portion of the target skull. Visual overlap was required between each sequential photo in the dataset, so the rig was manually rotated at approximately 5-degree increments. ReCap Photo, a part of Autodesk ReCap™ Pro, was used to generate a 3D model consisting of a polygonal mesh and texture map. The first process included errors, such as holes or inclusions of the target object's surroundings, so the generated mesh was brought into Autodesk Maya® for cleanup and UV map reconstruction. Finally, the model was imported into Mari by The Foundry (2020) for texture reprojection and color correction. Altogether, this workflow was much less time-consuming than established photogrammetric practices in archaeology and anthropology as their use of the orbiting rig alongside commercial 3D film software allowed for easier and more consistent photograph capture sessions and reduced the processing steps to create usable 3D models (Redford et al., 2020).

Omari et al. (2020) used a Samsung® Galaxy S8 model SM-G950F (Android version 9) equipped with a 12-megapixel camera that was held by an observer to capture the target objects of three Bone Clone® human skulls from four clockwise rotational

angles: 45°, 0°, -30°, and -90°. The commercial software Agisoft Metashape® was used to develop the 3D models from the 2D photographs as well as take the desired measurements. Known reference distances included in the image capture process were then used to scale the model prior to taking the fourteen selected interlandmark distances. Measurements were taken by four separate observers of varying experience in triplicate on the physical skull, CT derived model, and photogrammetrically derived model for comparison. The authors found strong intraclass correlation coefficients (above 0.980) between measurements regardless of method. They also found strong interclass correlations for the physical, CT scanning, and photogrammetry measurements. Overall, there was a range of 1 - 9 mm difference across the measurements for each skull per method. The authors concluded that digital photogrammetric modeling provides a cheaper alternative to other digital modeling techniques such as laser and CT scanning and provides comparable results to traditional direct methods of measurement (Omari et al., 2020).

Software

While software such as Agisoft Metashape® and Autodesk ReCap™ Pro, Maya®, and Mari are well designed and highly functional, repeated or continual use of these commercial softwares can be costly. Meshroom by AliceVision® is a Python based, free open-source software that is used to create 3D models from 2D photographs (AliceVision, 2018). It does this by using a feature detection method called the scale-invariant feature transform algorithm which extracts discriminative patches in a first

image that can be compared to discriminative patches of a second image irrespective of rotation, translation, and scale. The program then fuses all feature matches between images into tracks, each representing a point in space visible from multiple cameras. These multipoint views are then used to triangulate the 2D features into 3D points. The depth value of each pixel is then retrieved via Semi-Global Matching (SGM) which in essence takes overlapping planes of view from nearby cameras to create a volume W, H, Z depth candidates per pixel. The similarity for these points are then computed by the Zero Mean Normalized Cross-Correlation (ZNCC) of a small patch in the main image reprojected into the other camera and noise is filtered out. A refining step is then applied to get depth values with sub-pixel accuracy. Finally, a mesh and texture map are computed. The depth maps and compatible depth values are merged into the octree cells as a Delaunay tetrahedralization is performed. A Laplacian filtering on the mesh to remove local artifacts and bad cells are filtered on the surface. The texture map is computed by using visibility information associated with each vertex to retrieve the texture candidates and filter cameras without a good angle to the surface. The program outputs .mtl and .obj textured mesh files that are easily imported to 3D editing programs (Kneip et al., 2011).

Blender is also Python based and is a free open-source 3D creation suite capable of supporting the entirety of the 3D pipeline: modeling, rigging, animation, simulation, rendering, compositing, motion tracking, and even video editing and game creation (Foundation, 2022). Key features of Blender include mesh structure editing such as vertices, edges, faces, and topology, UV map editing, curve and object creation, edge

snapping, and curve to mesh converters (Blender Development Team, 2020). Both Meshroom and Blender are capable of customization through the creation of specialized tools and add-ons which can be used for specialized tasks. Tools and add-ons which other users have created are also widely available on the Blender website and other platforms such as GitHub. Both softwares are easy to use, available for download on any operating system with the minimum system requirements and have all features available at zero cost.

This study utilized a modified photogrammetric workflow based on those described in Omari et al. (2020) and Redford et al. (2020), primarily focusing on creating a simplified and low-cost method for 3D digitization that produces accurate and repeatable measurements for the os coxa. In order to accomplish this, free, open-source software has replaced the expensive commercial softwares used in the above studies. This study then tested the applicability of the curvature analysis described in Biwasaka et al. (2012) for accurate assigned sex estimation from the GSN on modern U.S. skeletal individuals from the Boston University Chobanian & Avedisian School of Medicine. Through this study, we sought to develop and streamline a cost-effective photogrammetric workflow and digital osteological analysis, demonstrating through the use of novel assigned sex estimation techniques the flexibility and applicability of the technique to anthropological and archaeological contexts.

MATERIALS AND METHODS

Photogrammetry

Os coxae of 12 adult individuals (53-92 years old) from the Boston University Chobanian & Avedisian School of Medicine Forensic Anthropology Program's Donated Skeletal Collection (with known demographics and provenance) and three anatomized adult individuals from the department of Anatomy and Neurobiology in the school of medicine (with unknown demographics and provenance) were utilized for this study. The left and right os coxae from each individual were treated as individual samples and analyzed separately, resulting in a total sample of 30 os coxae. The assigned sexes at birth of 12 donor individuals, five females and seven males, were documented and used as a baseline for the analysis of the sex estimation methodology utilized in this study. The estimated assigned sexes at birth of the three anatomized individuals, all estimated male, were based on pubic bone morphologies following Klales et al. (2012). Thus, the total sample consisted of 10 female and 20 male os coxae. The known or estimated sexes were not known until completion of the digital sex estimation to reduce bias.

Image quality and definition were essential for the creation of the models. A Fujifilm X-Pro2 and Fujifilm 35 mm prime lens mounted on a telescoping tripod were utilized during image capture (*FUJIFILM X-Pro2 | Cameras*, 2020; *FUJINON XF35mmF1.4 R | Lenses*, 2021). The target objects were placed on the Orangemonkie Foldio360 turntable and extension kit within the Foldio3 lightbox and full kit (*Foldio3,* 2021; *Foldio360 Smart Turntable,* 2021). To provide optimal detail capture, a black felt photographic background was used for heightened contrast between the os coxa and

negative space. Likewise, a matte black photographic paper was cut to size and wrapped around the turntable top. This contrast allows for easier recognition by the photogrammetric program between target object and background data when compiling the textured mesh. Lighting from the built-in lightbox as well as the additional halo lights were set via the android app to full brightness while the halo light on the turntable was set to 50%. The individual os coxae were oriented with the pubic symphysis facing downward and the ilium supported by 2-3 wooden dowels to raise it off the turntable's surface (Figure 1). The turntable rotation was also set via the app to 1x rotational speed which resulted in a 360 degree rotation in approximately 40 seconds. The camera interval shooting was set to one photograph per second for 41 captures to ensure adequate coverage of all angles. A full rotation was captured three times from three different angles for a total photographic dataset of 123 images. The camera was placed at approximately -45 degrees for the first rotation, 0 degrees or on a horizontal plane with the target objects for the second, and 45 degrees for the final capture. A photographic scale was included in the frame as well as a label which identified the item number and side of the body to which it belongs.

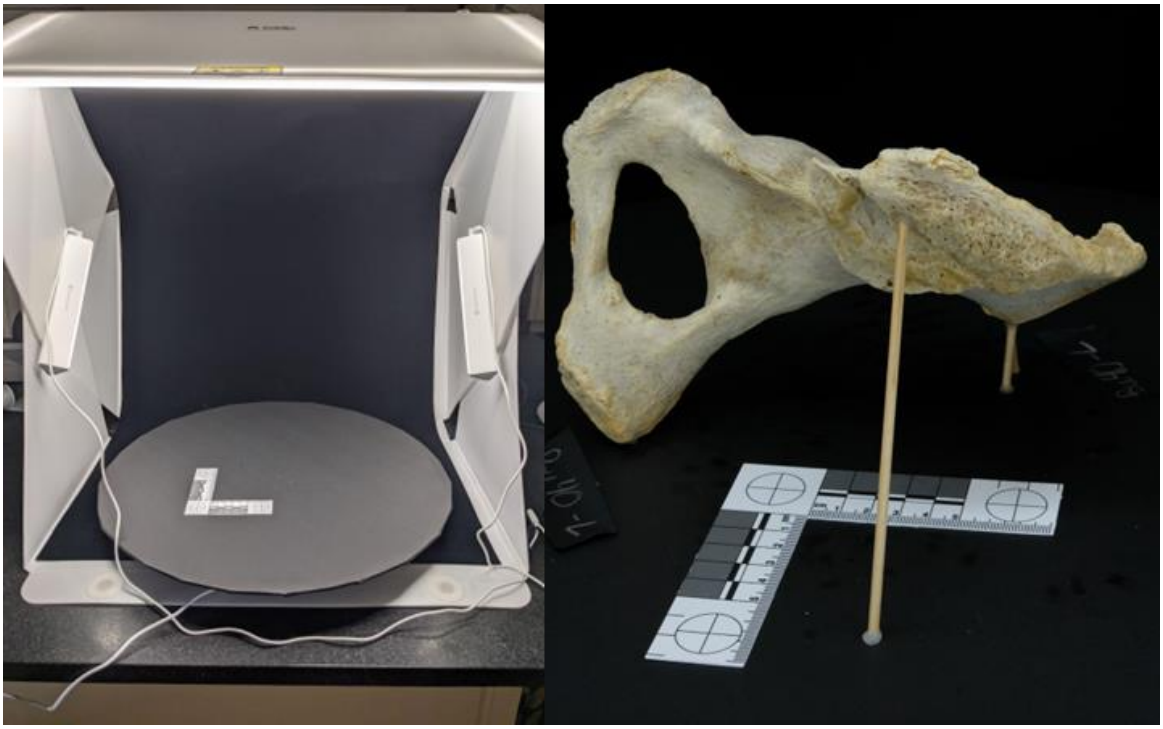

Figure 1. Photo capture setup (left) and BU40-L (right) with scale and wooden supports.

The photographs were then uploaded to a x64-based Windows 10 desktop computer for processing. The computer met the minimum system requirements for Meshroom and Blender. A hardware malfunction occurred with the motherboard of system 1 during the course of this project and was replaced along with the processor and GPU to form system 2 (Table 1). A Toshiba DT01ABA100V 1TB internal hard drive and a Seagate 1TB backup slim external hard drive were used for data storage and backup. Folders were created for each dataset and labeled using a convention of [ITEM#]-[SIDE]_[MMDDYY]. Meshroom, an open-source program, was used to convert the photographic datasets into a textured mesh or .obj file. The default settings for Meshroom were utilized and no adjustments were made to the node workflow. Each sample processed for approximately one to one and a half hours so a batch-run format (see Appendix A) was created and implemented in a windows command script such that

multiple samples could be queued and left to run without user management. The batch-run process also simultaneously created 'model' directories in each corresponding sample directories for easy data management. The samples were selected for the batch run by adding the desired folder names to separate lines in a text document titled samples-to-run.txt. Between four and six samples were selected at a time and left to process overnight. Using this methodology, the total of 28 textured meshes were completed within seven days.

	System 1	System 2
Processor	Intel® i7-6700	AMD Ryzen™ 9 5950X
GPU	MSI GeForce RTX 2070 Super	MSI GeForce RTX 3060 Ti
RAM	Corsair Vengeance 40.0 GB combined	GSkill Trident Z 64.0 GB combined
Motherboard	GIGABYTE GA-Z170X Gaming 3 ATX	ASUS ROG STRIX X570-E Gaming

Table 1. Comparison of system specifications utilized throughout data processing.

The completed textured meshes were found in …\model\MeshroomCache\Texturing\[###]\texturedMesh.obj and could be immediately imported into the second open-source mesh editing program, Blender. The model was then brought to the center of the 3D workspace and cleaned up in editor mode by removing extraneous vertices of the background and wooden supports used during data capture. Placing the viewport shading into wireframe mode allows for the selection of overlapping vertices for removal. The areas containing the photographic scale and item number were left intact. Once cleaned, the GSN was oriented such that it laid in the first quadrant of at least one of the 2D coordinate planes for ease of data processing. It was

ensured that the posterior inferior iliac spine (PIIS); ischial spine (IS); and the deepest point of the sciatic notch (DP) were in line on the same transverse coordinate plane (Figure 2).

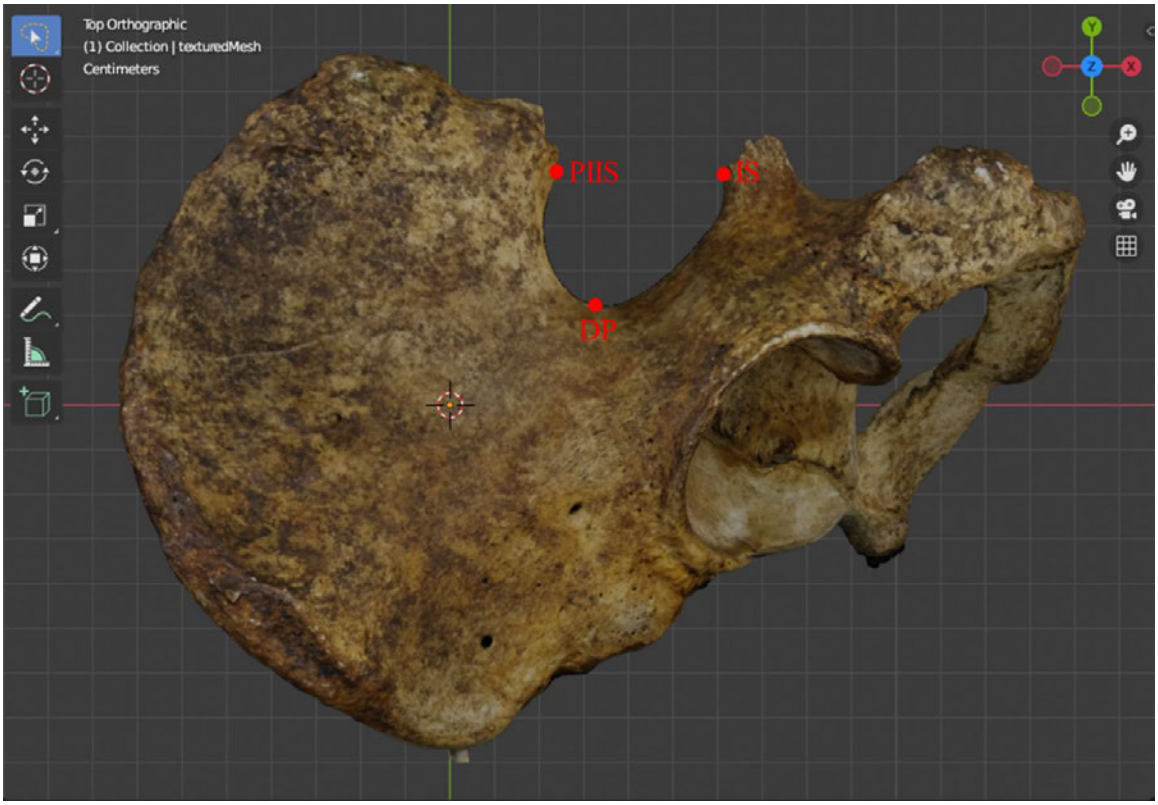

Figure 2. Orientation of the GSN of Individual BU35-L in an orthographic view such that the PIIS, DP, and IS are featured in the same plane.

Model Scaling

After model adjustment and orientation, a 1:1 global unit scale was applied. This was accomplished by utilizing the measurement tool to measure the photographic scale which was digitized alongside the os coxa. The units of the model were adjusted by selecting "scene properties," "units," and changing the length to millimeters. In the same tab, the known measurement of the photographic scale (50 mm) can be divided by the digital measurement (in mm) given by the measure tool in the "unit scale" section. This

changed the arbitrary scale of the model to a usable, real-world scale. The digital measurement of the photographic scale then reads the correct measurement of "50 mm."

In order to determine the accuracy of the resulting 3D mesh and usefulness for the acquisition of measurements, manual methods were used as a comparative baseline. Dry bone measurements of the os coxa height (OCH), superior iliac breadth (SIB), acetabular height (AH), and obturator foramen height (OFH) and breadth (OFB) were taken using sliding calipers and an osteometric board following White et al. (2012). The measurement tool was then used to take the same measurements digitally as they were taken on the dry bone. Several months after the initial measurements, a second set of dry bone and digital measurements were taken (Figure 3 and 4). Each measurement instance (dry measurements 1 and 2, and digital measurements 1 and 2) were compared against each other for error rates (i.e., difference between skeletal and model derived measurements) and variance through a linear regression model (R^2) between measurements of the same type (OCH, SIB, AH, OFB, and OFH).

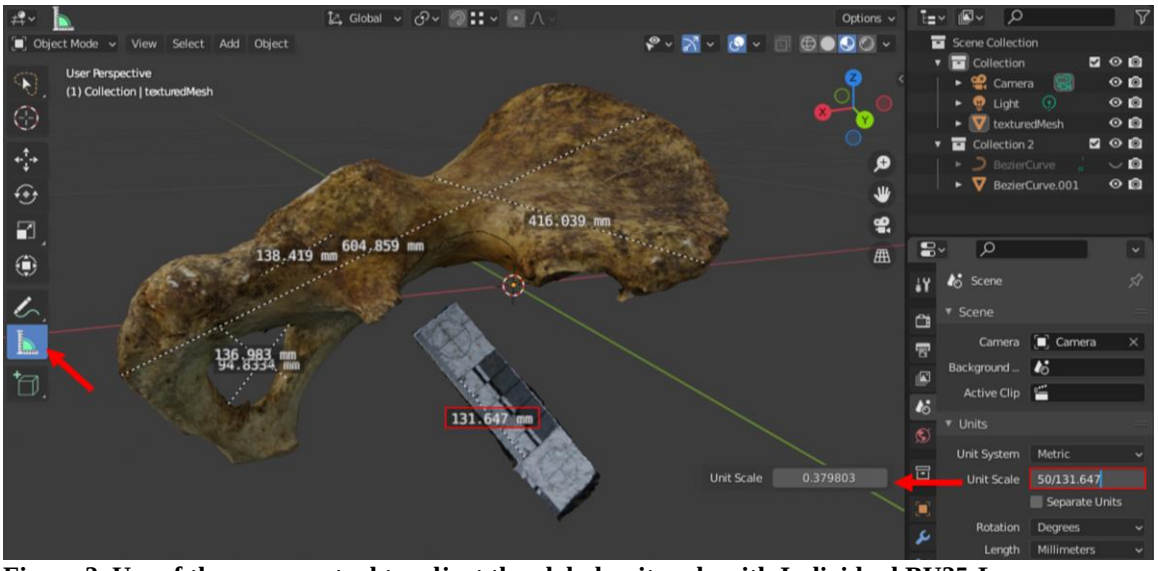

Figure 3. Use of the measure tool to adjust the global unit scale with Individual BU35-L.

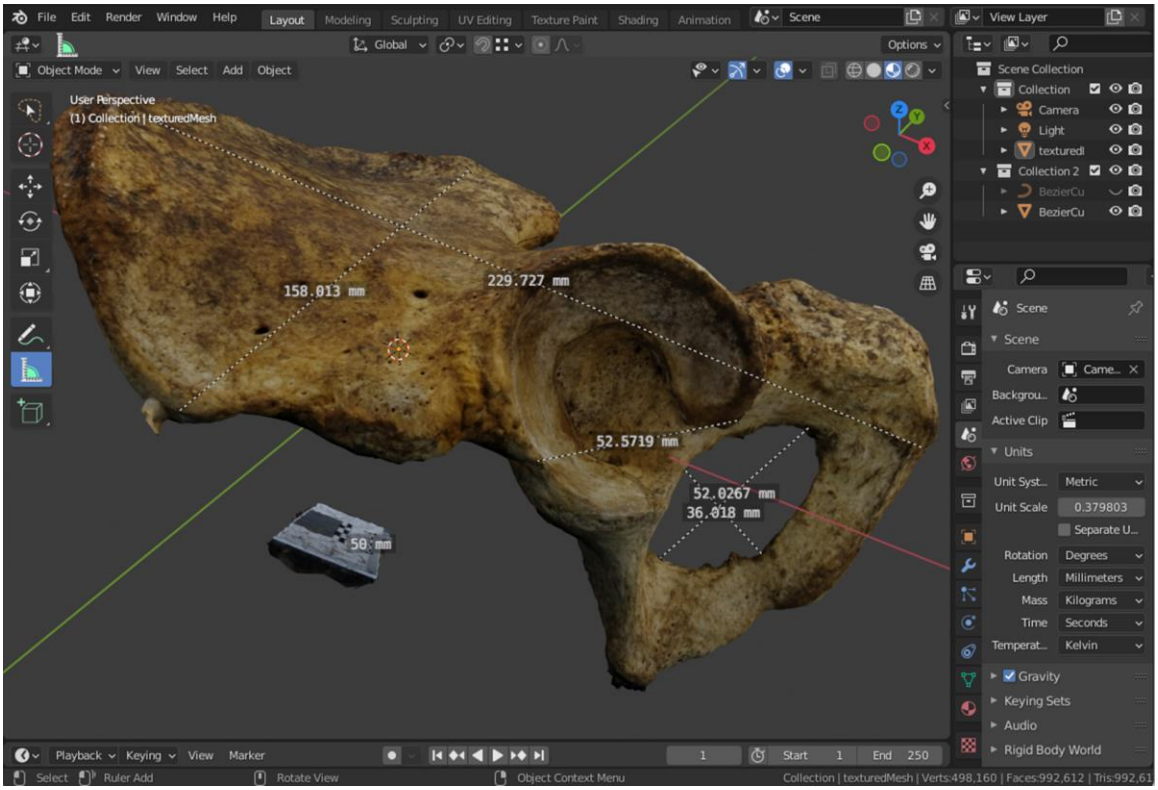

Figure 4. Digital measurements of the OCH, SIB, AH, OFH, and OFB of Individual BU35-L.

Assigned Sex Estimation

The 3D model was then brought into a perpendicular orthographic view to apply the spline curve to the outline of the GSN. This orthographic view is necessary to bring the 3D model into a 2D plane such that the outline of the GSN can be accurately viewed. The spline curve was created by first applying a Bezier curve to the workspace and attaching either end to the PIIS and IS using the control key such that the vertex of the curve locked to the edge of the mesh. In the editing mode, the curve arms of the end vertices were moved and adjusted to approximate the outline of the GSN. The "Curve Tools" add-on was used to measure the length of the Bezier curve, and it was adjusted until it is approximately 60 mm in length. The Bezier curve was then duplicated, and the

duplicate was converted into a mesh. The resulting mesh curve was then subdivided to create additional vertices and the curve was further adjusted to represent the desired outline. Once properly adjusted, the curve was further subdivided until a minimum of 1,000 vertices were achieved (Figure 5). The majority of vertices were concentrated in the deepest point of the GSN for adequate curvature representation.

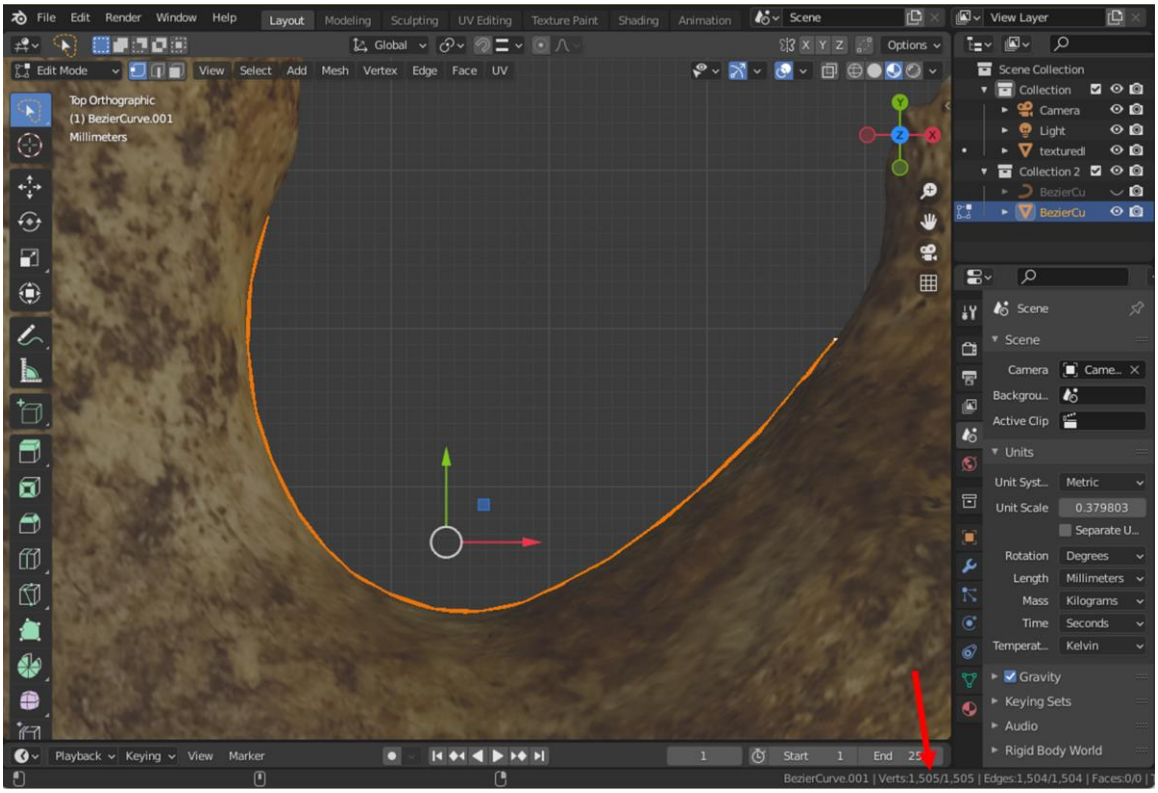

Figure 5. Mesh of the Bezier curve (orange line) of Individual BU35-L and number of vertices (bottom right red arrow).

The curve mesh was then exported using a custom add-on, "Curve to CSV Export Operator" (see Appendix B). The add-on compiles the global coordinate values of each vertex into a .CSV file which can then be easily utilized in statistical programs. Since the x, y, and z coordinates are exported indiscriminately, the "z" value of a single vertex was

manually set to zero prior to the export to indicate which column in the .CSV is unnecessary. The values exported from Blender are in reference to the global plane and the unit scale conversion factor created previously must be utilized in order to convert the units into the correct metric. Each value was multiplied by the same ratio found in the "unit scale" tab of blender to convert them into meters and further multiplied by 1000 to convert them into millimeters.

The .CSV files were then brought into the statistical program RStudio for computation of the best-fit circles. The functions utilized for calculating a best-fit circle for the data followed the least squares method described in Umbach and Jones (2003) (see Appendix C). The dataset was first defined as "xy" then run through the "fitSS" function to produce the parameters for the circle which was defined as data set "f." Among these data are the coordinates of the circle center and the radius. The circle and data were then plotted using the "circlexy" function to ensure that the circle produced passed through the deepest inflection point of the GSN as represented by the data (Figure 6).

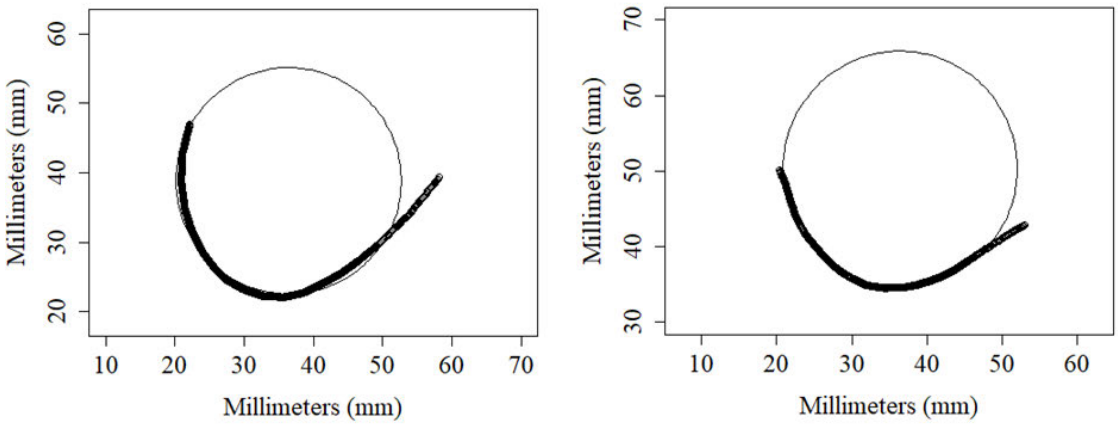

Figure 6. Best fit circles of Individual BU35-L (left) and Individual BU38-L (right).

The radius of the best-fit circle and height of the os coxa were then used to compute the curvature quotient ((radius/os coxa height)*100) for each sample following Biwasaka et al. (2012). The method was completed twice using the first and second set of digital measurements. The final assigned sex estimation was then achieved by utilizing the cutoff value of 7.6 for spline curves of 60 mm. Values above 7.6 were estimated to be female and below were estimated to be male. These estimations were then compared to the assigned or estimated sex for each available sample.

.

RESULTS

Evaluation of Reproducibility of Reconstructed 3D Models

Individuals BU37 and BU41 have fused os coxae and sacra, and the left os coxa and sacrum of Individual BU34 are fused. Thus, these individuals had to be digitized as single units and later digitally separated. Measurements from several samples such as the OCH and SIB from Individual BU30-L and the OFB from Individual BU30-R were unable to be taken due to extreme cortical bone loss and damage. The acetabular heights from Individuals BU32-L and BU33-L were also unable to be taken due to surgical implants. In each case, the DP and general shape of the GSN were unaffected. Surgical implants with lustrous or reflective components produced errors in the digital mesh of those areas; however, the errors were localized to the reflective surface and did not affect the overall mesh nor areas significant to the present study such as the GSN.

The two instances of dry bone measurements (dry 1 and 2) accomplished with manual tools and the two instances of digital bone measurements (dig. 1 and 2) accomplished in the program were compared in pairs across each measurement type. Measurements of the OCH produced an average error between 0.06% and 0.73% and R2 between 0.959 and 0.991 across comparisons (Tables 2 and 3). The first and second OCH digital measurements were the highest with an average 0.09% error, and R2=0.991 (Figure 7). Measurements from the OFB produced an average error between 0.19% and 3.48% and R2 between 0.673 and 0.856 across comparisons (Tables 2 and 3). The second dry measurements and first digital measurements were the lowest with an R2 of 0.673 and a 0.91% error (Figure 8). The resulting accuracy of digital measurements of the

sample was between 96.52% and 99.00%. Comparison of the first and second digital measurements resulted in the least percent error across the os coxa; 0.09% error for OCH, 0.19% for SIB, 0.20% for acetabular height, 0.22% for OFH, and 0.19% for OFB.

	Os Coxa Height	**Superior Iliac Breadth**	**Acetabular Height**	**Obturator Foramen Height**	**Obturator Foramen Breadth**
Dry 1 v 2	0.969	0.964	0.848	0.933	0.792
Dig. 1 v 2	0.991	0.941	0.874	0.932	0.856
Dry 1 v Dig. 1	0.973	0.952	0.842	0.749	0.808
Dry 1 v Dig. 2	0.959	0.926	0.787	0.793	0.706
Dry 2 v Dig. 1	0.983	0.924	0.781	0.807	0.673
Dry 2 v Dig. 2	0.984	0.947	0.774	0.861	0.691

Table 2. R^2 results for dry bone and digital measurement comparisons.

	Os Coxa Height	**Superior Iliac Breath**	**Acetabular Height**	**Obturator Foramen Height**	**Obturator Foramen Breadth**
Dry 1 v 2	0.06%	1.16%	1.20%	0.47%	1.49%
Digital 1 v 2	0.09%	0.19%	0.20%	0.22%	0.19%
Dry 1 v Digital 1	0.33%	0.38%	1.69%	0.90%	2.30%
Dry 1 v Digital 2	0.24%	0.57%	1.84%	0.99%	2.69%
Dry 2 v Digital 1	0.39%	0.79%	0.39%	1.28%	0.91%
Dry 2 v Digital 2	0.73%	0.71%	2.35%	2.46%	3.48%

Table 3. Average percent error rates for dry bone and digital measurement comparisons.

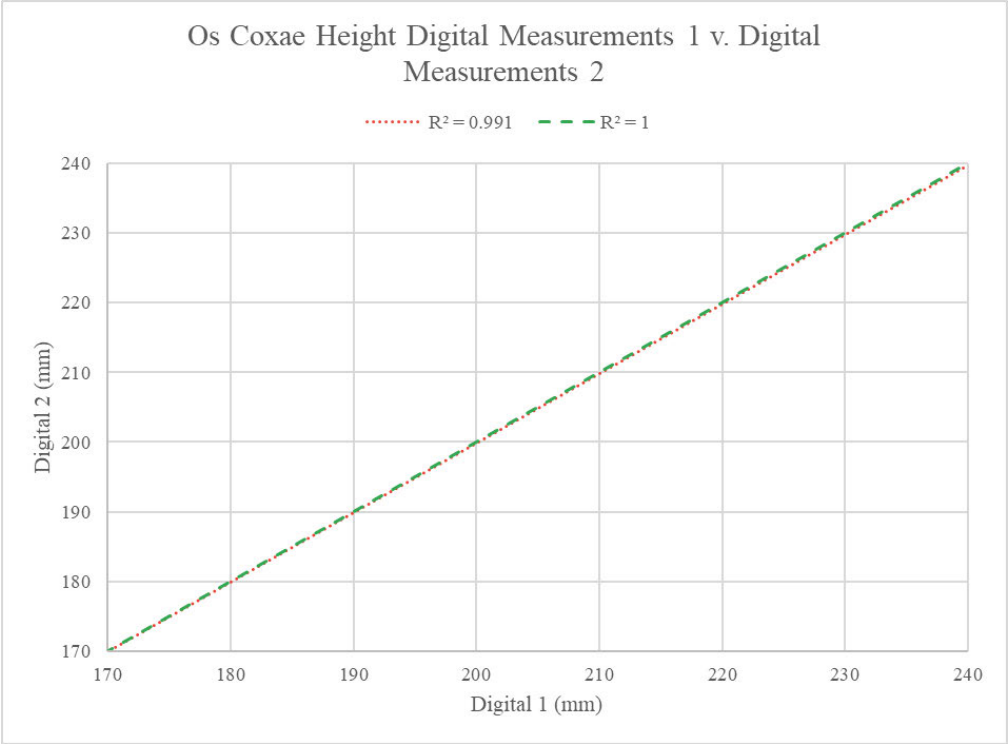

Figure 7. Comparison of digital measurements 1 and 2.

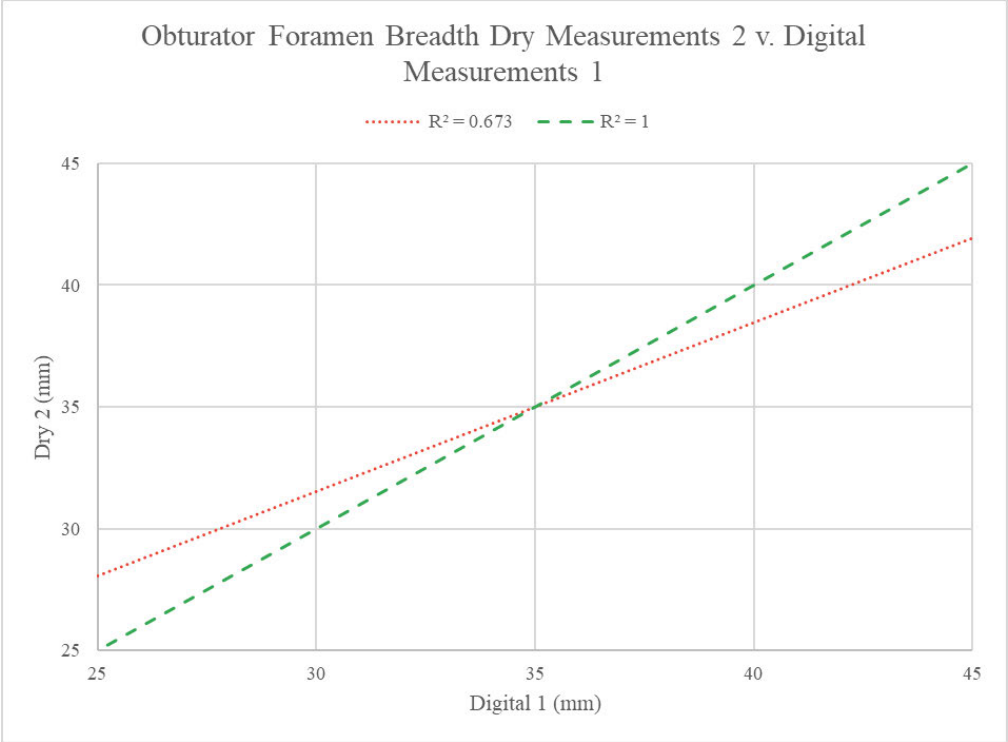

Figure 8. Comparison of dry measurements 2 and digital measurements 1.

Evaluation of Biological Sex Estimation from the GSN

Sex estimation of Individual BU30-L could not be completed due to damage to the superior iliac crest, which inhibited the measurement of the OCH and thus the curvature quotient could not be calculated. The assigned sex estimations following Biwasaka et al. (2012) achieved using either the first or second set of digital measurements matched the documented or pubic estimated sex of every individual. The digital sex estimations also matched the estimations following the techniques described in Walker (2005) for the individuals lacking documentation (Table 4).

Individual	**Radii**	**CQ from Dig. 1**	**Metric Estimation from Dig. 1**	**CQ from Dig. 2**	**Metric Estimation from Dig. 2**	**Walker (2005)**	**Known Sex**
BU30-R	22.925	10.768	Female	10.721	Female	Indeterminate	Female
BU31-L	12.795	5.781	Male	5.716	Male	Male	Male
BU31-R	14.132	6.359	Male	6.385	Male	Male	Male
BU32-L	14.342	7.769	Female	7.718	Female	Indeterminate	Female
BU32-R	15.642	8.459	Female	8.450	Female	Indeterminate	Female
BU33-L	18.992	9.145	Female	9.149	Female	Indeterminate	Female
BU33-R	19.583	9.613	Female	9.780	Female	Indeterminate	Female
BU34-L	14.108	5.962	Male	5.957	Male	Male	Male
BU34-R	9.493	3.963	Male	4.019	Male	Male	Male

BU35-L	16.281	7.090	Male	7.087	Male	Male	Male
BU35-R	15.023	6.554	Male	6.533	Male	Male	Male
BU36-L	17.234	7.382	Male	7.384	Male	Male	Male
BU36-R	15.272	6.662	Male	6.668	Male	Male	Male
BU37-L	16.332	7.595	Male	7.596	Male	Indeterminate	Male
BU37-R	13.133	6.020	Male	5.999	Male	Indeterminate	Male
BU38-L	15.581	8.050	Female	8.151	Female	Indeterminate	Female
BU38-R	16.095	8.309	Female	8.333	Female	Indeterminate	Female
BU39-L	13.483	6.008	Male	6.009	Male	Male	Male
BU39-R	11.313	5.060	Male	5.138	Male	Male	Male
BU40-L	17.975	8.771	Female	8.740	Female	Indeterminate	Female
BU40-R	17.817	8.836	Female	8.841	Female	Indeterminate	Female
BU41-L	13.169	6.029	Male	6.056	Male	Male	Male
BU41-R	14.423	6.544	Male	6.556	Male	Male	Male
BU3025-L	11.224	5.374	Male	5.361	Male	Male	N/A
BU3025-R	11.074	5.318	Male	5.322	Male	Male	N/A
N3943-L	14.516	6.176	Male	6.140	Male	Male	N/A
N3943-R	13.429	5.826	Male	5.829	Male	Male	N/A
N4238-L	14.880	7.071	Male	7.028	Male	Male	N/A
N4238-R	15.077	7.054	Male	7.042	Male	Male	N/A

Table 4. Radii; curvature quotients using the first and second sets of digital measurements; metric sex estimation following Biwasaka et al. (2012); estimated sex following Walker (2005); and known sex for the study sample. Metric sex estimation was established using a cutoff curvature quotient of 7.6 for a spline curve of 60 mm following Biwasaka et al. (2012). Curvature quotients above the cutoff were estimated as female and below the cutoff as male.

DISCUSSION

The present study developed and utilized photogrammetry and open-source softwares to produce 3D models for anthropological analysis. The resultant models exhibited a high level of surface detail, color, and texture when compared to other conventional methods of digitization such as CT scanning (see Figures 2-5). Measurements derived from the models were also highly accurate when compared to traditional dry bone methods with less than a 4% error rate, and most (63.3%) with less than a 1% error rate (see Table 3). The consistency between subsequent measurements of the same category (i.e., dry 1 vs 2 and dig. 1 vs 2) also increased with the use of the digital format, suggesting that this methodology can aid in reducing intra- and inter-observer error. This study also demonstrated the flexibility and applicability of photogrammetric derived models to forensic and osteological contexts through the application of novel and complex curvature analysis to the estimation of assigned sex at birth.

Successes and Limitations

The models created for this study far exceeded expectations with regards to the level of mesh detail and accurate representation of the selected elements. The accuracy of the 3D reconstructed elements depends on the quality and consistency of the photographic dataset. The use of a high-resolution digital camera in conjunction with the lightbox and turntable setup allowed for control and consistency between object capture sessions and replicability of optimal capture conditions. While the capture sessions

described in this research occurred in a lab setting, the portability of the folding lightbox and turntable allows for the photo-documentation process to be conducted in the field. The resulting meshes and textures from this technique were highly detailed and accurately visually represented the os coxae (Figure 9). Whereas CT scans are capable of examining surface topography to a degree and can be converted to 3D renderings (Kelley & Tallman, 2022), they are unable to capture the color or texture of the bone being scanned, which photogrammetry is capable of. However, in cases where reflective surgical hardware or metallic reconstructions were involved, the models exhibited various errors. The scale-invariant feature transformation algorithm utilized by Meshroom is often unable to feature-match on metallic or reflective surfaces as the reflection changes from angle to angle. As anthropological measurements are unable to be obtained from such areas even on dry bone, the errors had little to no effect on the results. A potential workaround exists in various commercial softwares such as 3DF Zephyr or Agisoft's Photoscan which have masking tools. These masking tools can be used to differentiate between foreground, background, and reflective surfaces to produce models without defects. At the time of this publication, there are adequate Meshroom workarounds available that users are collaboratively developing via Github (*Image Masking · Issue #188 · Alicevision/Meshroom*, 2022).

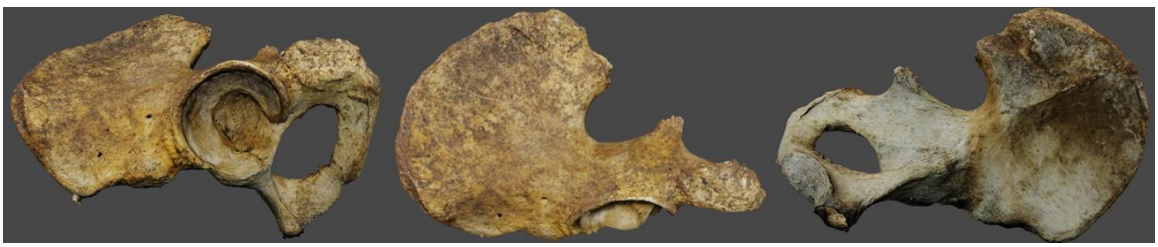

Figure 9. Textured mesh of BU35-L from the acetabular (left), lateral (middle), and medial (right) views.

This methodology was also found to be relatively quick and easy to accomplish as compared to CT scanning and processing. With the exclusion of the lightbox and camera setup (approximately 20 minutes), the image capture sessions required approximately 10 to 15 minutes per os coxa, allowing the full dataset of 30 os coxae to be completed in approximately 10 hours spread across several days. Each photographic dataset of 123 raw images then processed for approximately one and a half hours with the specifications of system 1, an hour or less with system 2, and required manual initiation to begin the processing of subsequent datasets (see Table 1). The batch-run process that was created for the Meshroom processing allowed for a degree of autonomous processing which could be left without researcher supervision while other tasks were accomplished or left to process overnight (see Appendix A). The model creation process in its entirety was accomplished in approximately seven days for all 30 os coxae. In Blender, with minimal program training, the model cleanup, digital measurement, and spline curve creation required approximately an hour per os coxa, which decreased to 30 minutes as shortcuts and quick keys were learned. Similarly, the application of an R package greatly reduced the assigned sex estimation process (see Appendix C). The creation of various program add-ons and plug-ins utilized in this study simplified the use of these open-source programs for anthropological application by researchers with little to no experience with the related softwares. Further professional customization of the softwares can better streamline the image capture and model creation process such that it can be easily applied to a variety of fields and applications such as repatriation, preservation, teaching, paleontology, and pathology (Carew et al., 2019, 2022; Grilli & Remondino, 2019;

Kakaliouras, 2012; Means, 2016; Moazen et al., 2013; Remondino, 2011, 2011; Schug et al., 2020; Vandenbossche et al., 2022; Ventola, 2014; Wachowiak & Karas, 2009).

The skeletal measurements achieved through this process produced no less than 96% consistency between measurement modalities and produced 100% accuracy for assigned sex estimation. These results mirror the successes of achieving accurate measurements from digital models in similar studies (Biwasaka et al., 2009; Carew et al., 2019; Omari et al., 2020; Placiente, 2017; Verhoff et al., 2008). Measurements of the os coxae height and superior iliac breadth proved the most accurate across samples with 98.84 - 99.94% consistency when compared to standardized dry bone measurements and between digital measurements. These areas of the os coxae were largely undamaged and free of interfering osteophytes, allowing the measurements to remain consistent across measurement modalities. Measurements of the obturator foramen height and breadth were less accurate with 96.52 - 99.81% accuracy across comparisons. The increased discrepancies between these measurements are likely a result of the presence of osteophytes in the obturator foramen of several of the older adults present in the sample. Similar osteophytes in the acetabula as well as a thickening of the bony margin of various individuals may have also affected the consistency between measurements. Interestingly, the least overall error of between 0.09% and 0.22% was achieved between the two instances of virtual measurements. The consistency of the measurements achieved with the virtual model increased when compared to the measurements achieved with the manual tools in all categories except for the os coxa height which decreased by a nominal amount of 0.03%. This suggests that the use of virtual measurement techniques allow for

increased intraobserver consistency as the arms of the measuring tool can be more precisely placed and locked as the other arm is adjusted. This eliminates the shifting and loss of positioning that can occur when utilizing handheld tools. These virtual measuring tools also allow for more precise placement of the measuring arms as the model can be freely rotated to fully visualize the desired placement on uneven surfaces such as in an obturator foramen on which osteophytes are present. The physical width of handheld tools can sometimes prevent appropriate placement and measurement of tight and uneven surfaces.

Application of the sex estimation techniques developed in Biwasaka et al. (2012) produced preliminary 100% success with this sample. The technique was developed using a contemporary Japanese sample, and the current research found no issues with applying the same method to photogrammetrically produced 3D models from a small, modern U.S. sample. Curvature analysis is not subject to the same limitations of other metric methods, which require undamaged landmarks. The deepest point of the GSN consists of relatively thick cortical bone and tends to survive in prolonged forensic and archaeological contexts whereas the posterior inferior iliac spine and posterior ischial spine are more easily damaged. This methodology therefore presents an alternative avenue for building a biological profile for highly fragmentary or damaged remains. Additionally, when compared to Walker (2005), a generally accepted method of assigned sex estimation, curvature analysis was found to be more nuanced. Following Walker (2005), all of the female os coxae and two of the male os coxae in the current study were classified as indeterminate (scores of 2). By comparison, there is no “indeterminate”

classification with Biwasaka et al.'s (2012) method, which allowed for the reduction of ambiguity with regards to the individuals with curvature quotients at or around the cutoff value. Due to limitations of travel and access to skeletal collections during the Covid-19 pandemic, the sample was limited to 30 os coxae and further testing with a larger sample and varying contemporary and historical groups is required before this technique can be fully validated as viable for utilization in forensic contexts. However, the success of adapting this technique to the 3D digitization methods and software available demonstrates the possibility of continued, more widespread use of this or similar digital methodologies for constructing aspects of the biological profile. While the majority of digitization research utilizes expensive CT equipment along with commercial software, the current research was able to successfully apply methods of measurement and assess assigned sex at little to no additional cost.

Future Directions

From the batch-run scenarios to purpose-built plug-ins and add-ons, the softwares utilized in this study can be applied to or used in the development of other anthropological techniques such as estimations for stature, population affinity, and age-at-death. Similarly, non-invasive reconstruction of fragmented elements and facial reconstruction can also be performed in a 3D virtual space. On 3D models of a skull, it is possible to identify cranial landmarks that can be used to estimate the population affinity and sex of the decedent and establish a foundation on which facial soft tissue thickness measurements can be selected and placed in the virtual space (Abdullah et al., 2022;

Cunha et al., 2021; Duke & Aguirre, 2010). Photogrammetry could also be applied in forensic contexts by law enforcement officers with minimal training (Omari et al., 2020). This can be especially useful in instances where an anthropologist has not yet arrived on-scene or where the remains are extremely fragile and can easily be damaged by environmental conditions, recovery, and transport.

This methodology can also be used to digitize entire collections to develop online databases. In such databases, it would be possible to compile files containing all available skeletal remains of an individual which are individually isolatable and measurable. Additionally, the provenance, biological data, and records of the individuals can be safely stored in the metadata of the files. For example, it would be possible to view the entirety of the remains in anatomical position or to view a specific element and perform measurements and research with all the necessary demographic information. This research could enable anthropologists to perform analyses of remains that they cannot have physical access to due to geographical constraints or unforeseen circumstances such as the global lockdowns which occurred as a result of the Covid-19 pandemic. Moreover, databases would enable anthropologists across the globe to collaborate with greater ease (Jiménez Fernández-Palacios et al., 2017; Minto & Remondino, 2014).

Such databases and open-source code could then be used to develop purpose-built anthropological programs. In instances of assigned sex estimation from the GSN, for example, machine learning and artificial intelligence (AI) could be taught to recognize desired features, such as the DP, PIIS, and IS or the outline of the GSN, from 2D and 3D images. The AI could then also be taught to apply various metric and nonmetric

techniques. Many free resources are currently available online to assist in building such a system. Amazon Web Services include a variety of free and paid machine learning services as well as free and paid cloud computational services (*Free Machine Learning Services - AWS*, 2023). This means that in the absence of a system that meets the minimum system requirements of the necessary software, a user could rent a virtual machine to perform those tasks in the cloud. Likewise, cloud processing could be useful in streamlining the model creation process as it is possible to rent a virtual machine with large capacity and Compute Unified Device Architecture (CUDA) capable video cards to potentially cut model creation time in half.

Many anthropologists have already begun the work to better understand the uses of 3D modeling and both open-source and commercial softwares in a variety of contexts (Osman & Tahar, 2016; Placiente, 2017; Redford et al., 2020; Remondino, 2011; Valenzuela & Julia, 2014; Vandenbossche et al., 2022; Winchester, 2016). The described method of digitization and assigned sex estimation need to be expanded to a larger sample size of more diverse demographics and populations. The method should also be applied to other skeletal elements of more complex development such as the cranium to test the success and accuracy of the digitization process with smaller and more varied structures and sutures. However, the anthropological community as a whole must also work to adapt institutional regulations to this rapidly expanding technological approach to protect the rights of the decedents and descendant communities and ensure the ethical and respectful use of the materials.

Ethical Considerations

The advent of novel methods of digital preservation and curation has highlighted the need for practitioners to formally consider the ethical principles with regards to the law, peoples, and communities with whom they work (Schug et al., 2020). Few institutional guidelines or civil laws currently govern the curation, transportation, destructive analysis, or public accessibility of human remains in the U.S. The laws and regulations that do exist are almost exclusively focused on Native American remains or on the prevention of disturbance of the recently dead (DeWitte, 2015; Ubelaker, 2011). This lack of ethical standards is perhaps most obvious in the field of digital curation (Hassett, 2018a, 2018b; Hirst et al., 2018; Ulguim, 2017, 2018; Wild, 2020; Wrobel et al., 2019). Public and academic institutions, such as museums and universities, often possess large collections of human remains in various states of preservation and accompanying information and from a variety of sources. Likewise, the methods, quality of, and resources for curation often differ between institutional bodies (Cassman et al., 2006). This diversity of circumstance lends to a complex discussion of the ethics involved and forces anthropologists to consider not only the anthropological ethics, but also the scientific ethics and bioethics (Schug et al., 2020).

Any discussion of ethics in skeletal biology requires an acknowledgement of the fact that biological and forensic anthropology are rooted in colonial and racist histories. Though the discipline has begun to develop an antiracist and anticolonial agenda (McCrane et al., 2022), much of the harm that has been caused by this history has yet to be addressed (Association of Black Anthropologists (ABA), 2021; Schug et al., 2020).

Early archaeological anatomical research was heavily influenced by Earnest Hooton (1887–1954) and Aleš Hrdlička (1869–1943), who were also strong proponents of "racial sciences" and eugenics (Buikstra & Beck, 2006). Similarly, the majority of the U.S.'s human skeletal collections utilized in anthropological research were assembled by privileged white scientists from the same time period who had few qualms about the collection of often marginalized deceased individuals to serve as anatomical specimens for teaching and research (de la Cova, 2019; DeWitte, 2015; Fabian, 2020; Knoeff & Zwijnenberg, 2016; Redman, 2016; Thomas, 2000). As a result, large reference collections of human remains were assembled through donations or were excavated from cemeteries and archaeological sites without the permission of those communities and with little to no consideration of the ethical dimensions of establishing, maintaining, or utilizing these collections over time. Though many institutional collections may be of known derivation, there are also a large percentage of remains which are unprovenanced for a variety of reasons. Further, until recently, there existed the commercial trade of human skeletal remains to the U.S. from South Asia which, generally speaking, are without adequate documentation and many of were sold without the knowledge or consent of the deceased individual or their families (Carney, 2007; Huffer & Chappell, 2014; Quigley, 2008). It was not until the last decades of the twentieth century that ethical practices regarding the obligations to the descendent communities, repatriation of mortuary remains through laws such as the Native American Graves Protection and Repatriation Act, or reflexivity about representation of people included in these collections as "others" in our discipline were put into widespread use (Kakaliouras, 2012;

Schug et al., 2020). As many work to establish ethical guidelines within the anthropological community, these guidelines likewise should address the use of new technologies, such as digital modeling and curation, as a basic launching point to ensure accountability and avoid further harm to antecedent and descendant communities.

As of 2019, the British Association of Biological Anthropology and Osteoarchaeology (BABAO) produced recommendations surrounding the ethical issues inherent in the 2D and 3D digital imaging of human remains. Among these recommendations surrounding preservation, digital sharing, analysis, and display and handling, the authors urge practitioners to consider how certain situational and individual conditions will affect the attempted use of the 2D or 3D imagery (Biers, 2019). Situational variables include the requirements resulting from consultation, legislation, and wider context which considers the local sensitivities and historical information. Individual variables relate to the identification or association with living groups, expressed wishes of the deceased, conditions of the remains, circumstances of death, and time since death (Alves-Cardoso & Campanacho, 2022; Ulguim, 2018). Schug et al. (2020) added to these suggestions 22 guidelines adapted from Cassman et al. (2006) to include recommendations about the use of the digital recreations in advertising, public education, teaching, and data storage. In most cases, institutional guidelines regarding the access and use of remains can be adapted for or extended to the digital recreations; however, the digital nature of the resources also poses unique challenges. In particular, Schug et al. (2020) discuss the efforts to identify appropriate repositories for the 3D scans of remains and whether it is appropriate to make the materials available to the public or

whether they should be restricted to academics and professionals in allied fields. While they support the idea of making such repositories available to the widest audience, they also recognize the potential misuse of the 3D scans if they are public, downloadable, and/or printable. In such cases, the authors recommend the implementation of a process that ensures that necessary access to the scans is fair and equitable. Similarly, the authors recommend against any advertising or commercial use of the scans, or any human remains. In cases of scientific outreach, such as to promote science literacy and STEM engagement activities, the authors stress that caution is still warranted in regard to respectful representation (Schug et al., 2020). While the present study demonstrates a cost effective and accurate way to realistically digitize human remains, we caution against the widespread digitization and sharing of human remains images without consultation with descendent communities or next of kin or with non-willed body donation collections. Moreover, while willed donors generally avail themselves to scientific study and teaching, we recommend that willed donation programs ask pre-donors whether they consent to having their remains digitized and widely shared.

CONCLUSION

The present study found that model derived osteological measurements were highly consistent and sufficient for anthropological use with less than a 4% error rate and with most (63.3%) with less than a 1% error rate. Additionally, the model derived measurements were more consistent between measurement sessions and indicate a reduction in inter- and intra-observer error when compared to traditional methods. Sex estimation via curvature analysis of the GSN achieved 100% accuracy and was found to be more nuanced than Walker's (2005) ordinal scoring method, as there are no indeterminate classifications. With the advancements in imaging and data processing technologies, the production of 3D models via photogrammetric methods has become affordable and widely accessible regardless of modeling experience. Decent quality cameras are almost ubiquitous in any anthropologist's toolbox and, as Omari et al. (2020) demonstrated, modern smartphone cameras have become nearly as powerful and ubiquitous. The present research utilized free, open-source softwares to produce accurate and highly detailed models that are comparable to physical measurements and demonstrated that it was a reliable and repeatable method. Additionally, with the added plug-ins, the software was simplified and does not require specialized knowledge nor extensive training to use effectively. It further demonstrated that complex curvature analyses for assigned sex estimation of the GSN could be successfully adapted and applied with the available methodology and sample. As such, this study streamlined the digitization and sex estimation process, demonstrating the high flexibility and

customization capabilities of the open-source programs for hyper-specialized anthropological use.

The application of methodologies developed in this research enables anthropologists to perform analyses on remains that they cannot access physically due to geographical or situational constraints. Additionally, it would allow anthropologists to collaborate with greater ease across distances and disciplines. In situ anthropological remains and their contexts could also be documented with ease in the field by any individual with a good resolution camera and basic direction in how to appropriately capture the photographs needed for the reconstruction. As such, it can supplement the preservation of fragile remains that can be altered or damaged during the excavation and collection processes. The application of the technique could also reduce the risk of damage as a result of repeated handling or examination of historical and fragile remains. While photogrammetry provides numerous research, collaboration, and curation benefits, such methodology is accompanied by unique ethical concerns that prevent it from simply replacing skeletal collections that were established unethically and include marginalized individuals.

APPENDIX A

Batch-run Command

```
@echo off
@setlocal
@setlocal ENABLEEXTENSIONS
@setlocal ENABLEDELAYEDEXPANSION

set MESHROOM="D:\Program Files\Meshroom-2021.1.0-win64\Meshroom-
2021.1.0\meshroom_batch.exe"
set THISDIR=%CD%

echo THISDIR = %THISDIR%

set SAMPLESFILE=samples-to-run.txt

if not exist %SAMPLESFILE% goto NOFILE

for /f %%s in (%SAMPLESFILE%) do (
  echo !!!=== %%s - Processing begins ===
  set IMAGESDIR=%THISDIR%\%%s
  cd "!IMAGESDIR!"
  if not exist model\MeshroomCache mkdir model\MeshroomCache
  cd model
  cd
  echo %MESHROOM% -p photogrammetry -i "!IMAGESDIR!" --save "%%s.mg" --
cache "!IMAGESDIR!\model\MeshroomCache"
  %MESHROOM% -p photogrammetry -i "!IMAGESDIR!" --save "%%s.mg" --cache
"!IMAGESDIR!\model\MeshroomCache"
)

goto :EOF

:NOFILE
echo.
echo ERROR can't find file samples-to-run.txt
echo.
echo aborting!
```

APPENDIX B

Blender Add-on: “Curve to CSV” Exporter

```
import bpy, bmesh
import csv

from bpy.types import Operator
from datetime import datetime
from os import path


bl_info = {
  "name": "Export Curve to CSV",
  "author": "Lance Carriere <lance@visiondriven.com",
  "version": (1, 3),
  "blender": (2, 93, 5),
  "description": "Export the selected curve verticies to CSV file",
  "category": "Object",
}

def write_some_data(context):

    thisFile = bpy.data.filepath
    now = datetime.today().strftime('-%Y%m%d-%H%M%S') # -20211009-141333
    path_output_csv = path.splitext(thisFile)[0] + now + '.csv'

    print(f'<-- STARTING OUTPUT TO {path.basename(path_output_csv)} -->')

    # get current selected object
    if len(context.selected_objects) != 1:
        print(f'{path.basename(__file__)} :: select 1 and only 1 mesh')
        ShowMessageBox(f'{path.basename(__file__)} :: select 1 and only 1 mesh')

        return False

    obj = context.active_object

    # got vertices?
    if obj.type != 'MESH':
        print(f'{path.basename(__file__)} :: selected object does not have vertices')
        ShowMessageBox(f'{path.basename(__file__)} :: selected object does not have
vertices')
        return False
```

```
import bpy, bmesh
import csv

from bpy.types import Operator
from datetime import datetime
from os import path

bl_info = {
 "name": "Export Curve to CSV",
 "author": "Lance Carriere <lance@visiondriven.com",
 "version": (1, 3),
 "blender": (2, 93, 5),
 "description": "Export the selected curve verticies to CSV file",
 "category": "Object",
}

def write  some  data(context):

  thisFile = bpy.data.filepath
  now = datetime.today().strftime('-%Y%m%d-%H%M%S') # -20211009-141333
  path  output  csv = path.splitext(thisFile)[0] + now + '.csv'

  print(f'<-- STARTING OUTPUT TO {path.basename(path  output  csv)} -->')

  # get current selected object
  if len(context.selected_objects) != 1:
    print(f'{path.basename(    file    )} :: select 1 and only 1 mesh')
    ShowMessageBox(f'{path.basename(__file__)} :: select 1 and only 1 mesh')

    return False

  obj = context.active_object

  # got vertices?
  if obj.type != 'MESH':
    print(f'{path.basename(__file__)} :: selected object does not have vertices')
    ShowMessageBox(f'{path.basename(    file    )} :: selected object does not have
vertices')
    return False

  # Get the Object via the blender API
```

```
  if obj.mode == 'EDIT':
    # this works only in edit mode,
    bm = bmesh.from_edit_mesh(obj.data)
    verts = [vert.co for vert in bm.verts]

  else:
    # this works only in object mode,
    verts = [vert.co for vert in obj.data.vertices]

  # coordinates as tuples
  plain_verts = [vert.to_tuple() for vert in verts]

  # output to CSV
  with open(path_output_csv, "w") as csvfile:

    vertWriter = csv.writer(csvfile, dialect='excel', lineterminator='\n')

    vertWriter.writerows(plain_verts) # squirt out all at once - yay


  print(f'\nCSV successfully created:\n{path_output_csv}')


  return path_output_csv

def ShowMessageBox(message = "", title = "Message Box", icon = 'INFO'):

  def draw(self, context):
    self.layout.label(text=message)

  bpy.context.window_manager.popup_menu(draw, title = title, icon = icon)

class ExportCurveToCSV(Operator):
  """Export the selected curve verticies to CSV file"""
  bl_idname = "export.curve_to_csv"  # important since its how
bpy.ops.import_test.some_data is constructed
  bl_label = "Export Curve to CSV"

  def execute(self, context):
    # return write_some_data(context)
    result = write_some_data(context)
    if result != False:
```

```
      self.report({'INFO'}, f'Vertices save to {result}!')
      ShowMessageBox(result, 'Vertices saved to:')
      return {'FINISHED'}
    else:
      return {'CANCELLED'}


# Only needed if you want to add into a dynamic menu
def menu_func_export(self, context):
  self.layout.operator(ExportCurveToCSV.bl_idname, text="Curve vertices to CSV
Export")

def register():
  bpy.utils.register_class(ExportCurveToCSV)
  bpy.types.TOPBAR_MT_file_export.append(menu_func_export)

def unregister():
  bpy.utils.unregister_class(ExportCurveToCSV)
  bpy.types.TOPBAR_MT_file_export.remove(menu_func_export)

if __name__ == "__main__":
  register()

  # test call
  # bpy.ops.export.curve_to_csv('INVOKE_DEFAULT')
```

APPENDIX C

RStudio Best Fit Circle Functions

```
fitSS <- function(xy,
                  a0=mean(xy[,1]),
                  b0=mean(xy[,2]),
                  r0 = mean(sqrt((xy[,1]-a0)^2 + (xy[,2]-b0)^2)),
                  ...){
   SS <- function(abr){
      sum((abr[3] - sqrt((xy[,1]-abr[1])^2 + (xy[,2]-abr[2])^2))^2)
   }
   optim(c(a0,b0,r0), SS, ...)
}


circlexy <- function(xyr, n=180){
   theta = seq(0,2*pi,len=n)
   cbind(xyr[1] + xyr[3]*cos(theta),
         xyr[2] + xyr[3]*sin(theta)
         )
}
```

BIBLIOGRAPHY

Abdullah, J. Y., Moraes, C., Rajion, Z. A., Hadi, H., Shahidan, S., Malin Abdullah, J., & Saidin, M. (2022). Forensic Facial Approximation of 5000-Year-Old Female Skull from Shell Midden in Guar Kepah, Malaysia. *Applied Sciences*, *12*(15), 7871. https://doi.org/10.3390/app12157871

Agisoft. (2020). *Agisoft Metashape* (1.8.4). https://www.agisoft.com/downloads/installer/

AliceVision. (2018). *Meshroom: A 3D reconstruction software.* https://github.com/alicevision/meshroom

Alves-Cardoso, F., & Campanacho, V. (2022). To Replicate, or Not to Replicate? The Creation, Use, and Dissemination of 3D Models of Human Remains: A Case Study from Portugal. *Heritage*, *5*(3), Article 3. https://doi.org/10.3390/heritage5030085

Association of Black Anthropologists (ABA). (2021, April 28). *Concerning the Possession and Unethical Use of the Remains of the Children of MOVE and the Africa Family: A Collective Statement from the Association of Black Anthropologists (ABA), the Society of Black Archaeologists (SBA), and the Black in Bioanthropology Collective (BiBA)*. https://aba.americananthro.org/collective-statement-concerning-the-possession-and-unethical-use-of-remains/

Autodesk, INC. (2021a). *Maya* (Version 2020). https:/ autodesk.com/maya

Autodesk, INC. (2021b). *Recap Pro* (Version 2020). https:/ autodesk.com/recap

Biers, T. (2019). *BABAO recommendations on the ethical issues surrounding 2D and 3D digital imaging of human remains 2019 2*. https://www.academia.edu/43667679/BABAO_recommendations_on_the_ethical_issues_surrounding_2D_and_3D_digital_imaging_of_human_remains_2019_2

Biwasaka, H., Aoki, Y., Sato, K., Tanijiri, T., Fujita, S., Dewa, K., Yoshioka, K., & Tomabechi, M. (2012). Analyses of sexual dimorphism of reconstructed pelvic computed tomography images of contemporary Japanese using curvature of the greater sciatic notch, pubic arch and greater pelvis. *Forensic Science International*, *219*(1), 288.e1-288.e8. https://doi.org/10.1016/j.forsciint.2011.11.032

Biwasaka, H., Aoki, Y., Tanijiri, T., Sato, K., Fujita, S., Yoshioka, K., & Tomabechi, M. (2009). Analyses of sexual dimorphism of contemporary Japanese using reconstructed three-dimensional CT images – Curvature of the best-fit circle of the greater sciatic notch. *Legal Medicine*, *11*, S260–S262. https://doi.org/10.1016/j.legalmed.2009.02.052

Blender Development Team. (2020). *Blender (Version 3.31 LTS)*. https://www.blender.org/

Buikstra, J. E., & Beck, L. A. (Eds.). (2006). *Bioarchaeology: The Contextual Analysis of Human Remains*. Routledge. https://doi.org/10.4324/9781315432939

Buikstra, J. E., & Ubelaker, D. (1994). *Standards for Data Collection from Human Skeletal Remains*. /paper/Standards-for-Data-Collection-from-Human-Skeletal-Buikstra-Ubelaker/7cd7439d34ed49c37cd878d0d253f3d655c4d036

Bytheway, J. A., & Ross, A. H. (2010). A Geometric Morphometric Approach to Sex Determination of the Human Adult Os Coxa. *Journal of Forensic Sciences*, *55*(4), 859–864. https://doi.org/10.1111/j.1556-4029.2010.01374.x

Carew, R. M., Iacoviello, F., Rando, C., Moss, R. M., Speller, R., French, J., & Morgan, R. M. (2022). A multi-method assessment of 3D printed micromorphological osteological features. *International Journal of Legal Medicine*, *136*(5), 1391–1406. https://doi.org/10.1007/s00414-022-02789-y

Carew, R. M., Morgan, R. M., & Rando, C. (2019). A Preliminary Investigation into the Accuracy of 3D Modeling and 3D Printing in Forensic Anthropology Evidence Reconstruction,. *Journal of Forensic Sciences*, *64*(2), 342–352. https://doi.org/10.1111/1556-4029.13917

Carney, S. (2007, November 29). Into the Heart of India's Underground Bone Trade. *NPR*. https://www.npr.org/2007/11/29/16678816/into-the-heart-of-indias-underground-bone-trade

Cassman, V., Odegaard, N., & Powell, J. (2006). *Human Remains: Guide for Museums and Academic Institutions*. Rowman Altamira.

Church, E. (2019). *The forensic utility of photogrammetry in surface scene documentation*. https://open.bu.edu/handle/2144/38598

Clemente, C. (1985). *Gray's Anatomy of the Human Body* (30th edition). Lea & Febiger.

Cunha, H. S., da Costa Moraes, C. A., de Faria Valle Dornelles, R., & da Rosa, E. L. S. (2021). Accuracy of three-dimensional virtual simulation of the soft tissues of the face in OrtogOnBlender for correction of class II dentofacial deformities: An uncontrolled experimental case-series study. *Oral and Maxillofacial Surgery*, *25*(3), 319–335. https://doi.org/10.1007/s10006-020-00920-0

de la Cova, C. (2019). Chapter 7 - Marginalized bodies and the construction of the Robert J. Terry anatomical skeletal collection: A promised land lost. In M. L. Mant & A.

J. Holland (Eds.), *Bioarchaeology of Marginalized People* (pp. 133–155). Academic Press. https://doi.org/10.1016/B978-0-12-815224-9.00007-5

DeWitte, S. N. (2015). Bioarchaeology and the Ethics of Research Using Human Skeletal Remains. *History Compass*, *13*(1), 10–19. https://doi.org/10.1111/hic3.12213

Duke, E. H., & Aguirre, S. R. (Eds.). (2010). *3D Imaging: Theory, Technology and Applications* (UK ed. edition). Nova Science Pub Inc.

Fabian, A. (2020). *The Skull Collectors: Race, Science, and America's Unburied Dead*. University of Chicago Press. https://press.uchicago.edu/ucp/books/book/chicago/S/bo5820708.html

Foldio3. (2021). ORANGEMONKIE – Simple, but Useful. https://us.orangemonkie.com/product/foldio3/

Foldio360 Smart Turntable. (2021). ORANGEMONKIE – Simple, but Useful. https://us.orangemonkie.com/product/foldio360-3/

Foundation, B. (2022). About Blender. *Blender.Org*. https://www.blender.org/about/

Free Machine Learning Services—AWS. (2023). Amazon Web Services, Inc. https://aws.amazon.com/free/machine-learning/

FUJIFILM X-Pro2 | Cameras. (2020). FUJIFILM X Series & GFX – Global. https://fujifilm-x.com/global/products/cameras/x-pro2/

FUJINON XF35mmF1.4 R | Lenses. (2021). FUJIFILM X Series & GFX – Global. https://fujifilm-x.com/global/products/lenses/xf35mmf14-r/

Gómez-Valdés, J. A., Quinto-Sánchez, M., Menéndez Garmendia, A., Veleminska, J., Sánchez-Mejorada, G., & Bruzek, J. (2012). Comparison of methods to determine sex by evaluating the greater sciatic notch: Visual, angular and geometric morphometrics. *Forensic Science International*, *221*(1), 156.e1-156.e7. https://doi.org/10.1016/j.forsciint.2012.04.027

Gonzalez, P. N., Bernal, V., & Perez, S. I. (2009). Geometric morphometric approach to sex estimation of human pelvis. *Forensic Science International*, *189*(1), 68–74. https://doi.org/10.1016/j.forsciint.2009.04.012

Grilli, E., & Remondino, F. (2019). Classification of 3D Digital Heritage. *Remote Sensing*, *11*(7). https://doi.org/10.3390/rs11070847

Hassett, B. R. (2018a). The Ethical Challenge of Digital Bioarchaeological Data. *Archaeologies*, *14*(2), 185–188. https://doi.org/10.1007/s11759-018-9348-8

Hassett, B. R. (2018b). Which Bone to Pick: Creation, Curation, and Dissemination of Online 3D Digital Bioarchaeological Data. *Archaeologies*, *14*(2), 231–249. https://doi.org/10.1007/s11759-018-9344-z

Hirst, C. S., White, S., & Smith, S. E. (2018). Standardisation in 3D Geometric Morphometrics: Ethics, Ownership, and Methods. *Archaeologies*, *14*(2), 272–298. https://doi.org/10.1007/s11759-018-9349-7

Huffer, D., & Chappell, D. (2014). The mainly nameless and faceless dead: An exploratory study of the illicit traffic in archaeological and ethnographic human remains. *Crime, Law and Social Change*, *62*(2), 131.

Image masking · Issue #188 · alicevision/Meshroom. (2022). GitHub. https://github.com/alicevision/Meshroom/issues/188

Jani, G., Johnson, A., Parekh, U., Thompson, T., & Pandey, A. (2020). Effective approaches to three-dimensional digital reconstruction of fragmented human skeletal remains using laser surface scanning. *Forensic Science International: Synergy*, *2*, 215–223. https://doi.org/10.1016/j.fsisyn.2020.07.002

Jiménez Fernández-Palacios, B., Morabito, D., & Remondino, F. (2017). Access to complex reality-based 3D models using virtual reality solutions. *Journal of Cultural Heritage*, *23*, 40–48. https://doi.org/10.1016/j.culher.2016.09.003

Johnson, A., Jani, G., Garriga, J. A., & Pandey, A. (2020). Digital reconstruction of fragmented tooth remains in forensic context. *Forensic Sciences Research*, 1–6. https://doi.org/10.1080/20961790.2020.1737462

Kakaliouras, A. M. (2012). An Anthropology of Repatriation: Contemporary Physical Anthropological and Native American Ontologies of Practice. *Current Anthropology*, *53*(S5), S210–S221. https://doi.org/10.1086/662331

Kelley, S. R., & Tallman, S. D. (2022). Population-Inclusive Assigned-Sex-at-Birth Estimation from Skull Computed Tomography Scans. *Forensic Sciences*, *2*(2), Article 2. https://doi.org/10.3390/forensicsci2020024

Khomiakov, I. S., Salamov, R. F., & Semenova, N. A. (1987). Age-related dynamics of the shape and size of the subpubic angle in children and adolescents. *Arkhiv Anatomii, Gistologii I Embriologii*, *93*(7), 47–51.

Kim, D.-H., Lee, S.-H., Lee, S.-S., Kim, Y.-S., Park, D.-K., Han, S.-H., & Lee, U.-Y. (2018). Comprehensive evaluation of the greater sciatic notch for sexual estimation through three-dimensional metric analysis using computed tomography based models. *Legal Medicine*, *35*, 1–8. https://doi.org/10.1016/j.legalmed.2018.09.006

Klales, A. R., Ousley, S. D., & Vollner, J. M. (2012). A revised method of sexing the human innominate using Phenice's nonmetric traits and statistical methods. *American Journal of Physical Anthropology*, *149*(1), 104–114. https://doi.org/10.1002/ajpa.22102

Kneip, L., Scaramuzza, D., & Siegwart, R. (2011). A novel parametrization of the perspective-three-point problem for a direct computation of absolute camera position and orientation. *CVPR 2011*, 2969–2976. https://doi.org/10.1109/CVPR.2011.5995464

Knoeff, R., & Zwijnenberg, R. (2016). *The Fate of Anatomical Collections*. Routledge. https://doi.org/10.4324/9781315558202

Koutsoudis, A., Vidmar, B., & Arnaoutoglou, F. (2013). Performance evaluation of a multi-image 3D reconstruction software on a low-feature artefact. *Journal of Archaeological Science*, *40*(12), 4450–4456. https://doi.org/10.1016/j.jas.2013.07.007

Kuzminsky, S. C., & Gardiner, M. S. (2012). Three-dimensional laser scanning: Potential uses for museum conservation and scientific research. *Journal of Archaeological Science*, *39*(8), 2744–2751. https://doi.org/10.1016/j.jas.2012.04.020

McCrane, S. M., Hsiao, C. J., & Tallman, S. D. (2022). Implementing an antiracist framework in forensic anthropology: Our responsibility in professional organizations and as scientists. *American Anthropologist*, *124*(3), 575–579. https://doi.org/10.1111/aman.13754

Means, B. (2016). *Virtual Mobility Archaeology Project With Further Applications of Three Dimensional Digital Scanning of Archaeological Objects Project # 13-334*. https://www.academia.edu/28265361/Virtual_Mobility_Archaeology_Project_With_Further_Applications_of_Three_Dimensional_Digital_Scanning_of_Archaeological_Objects_Project_13_334

Minto, S., & Remondino, F. (2014). Online access and sharing of reality-based 3d models. *SCIRES-IT - SCIentific RESearch and Information Technology*, *4*(2), Article 2. https://doi.org/10.2423/i22394303v4n2p17

Moazen, M., Costantini, D., & Bruner, E. (2013). A Sensitivity Analysis to the Role of the Fronto-Parietal Suture in Lacerta Bilineata: A Preliminary Finite Element Study. *The Anatomical Record*, *296*(2), 198–209. https://doi.org/10.1002/ar.22629

Nakao, T. (1998). A morphological study of the fetal ilium; focusing on the sexual differences of the greater sciatic notch. *Fukuoka Igaku Zasshi = Hukuoka Acta Medica*, *89*(2), 56–63.

NextEngine 3D Laser Scanner. (2020). NextEngine Store. https://www.nextengine.com/store

Omari, R., Hunt, C., Coumbaros, J., & Chapman, B. (2020). Virtual anthropology? Reliability of three-dimensional photogrammetry as a forensic anthropology measurement and documentation technique. *International Journal of Legal Medicine*, *135*(3), 939–950. https://doi.org/10.1007/s00414-020-02473-z

Osman, M. R., & Tahar, K. N. (2016). 3D accident reconstruction using low-cost imaging technique. *Advances in Engineering Software*, *100*, 231–237. https://doi.org/10.1016/j.advengsoft.2016.07.007

Patterson, M. M., & Tallman, S. D. (2019). Cranial and Postcranial Metric Sex Estimation in Modern Thai and Ancient Native American Individuals. *Forensic Anthropology*, *2*(4), 233–253. https://doi.org/10.5744/fa.2019.1009

Peckmann, T. R., Orr, K., Meek, S., & Manolis, S. K. (2015). Sex determination from the talus in a contemporary Greek population using discriminant function analysis. *Journal of Forensic and Legal Medicine*, *33*, 14–19. https://doi.org/10.1016/j.jflm.2015.03.011

Perrone, R. V., & Williams, J. L. (2019). Dimensional accuracy and repeatability of the NextEngine laser scanner for use in osteology and forensic anthropology. *Journal of Archaeological Science: Reports*, *25*, 308–319. https://doi.org/10.1016/j.jasrep.2019.04.012

Phenice, T. W. (1969). A newly developed visual method of sexing the os pubis. *American Journal of Physical Anthropology*, *30*(2), 297–301. https://doi.org/10.1002/ajpa.1330300214

Placiente, B. (2017). *The Identifiability of Osteological Traits on 3D Models of Human Skeletal Remains.* https://doi.org/10.13140/RG.2.2.29365.68322

Quigley, C. (2008). *Skulls and Skeletons: Human Bone Collections and Accumulations* (1st edition). McFarland.

Redford, A., Mikulski, R., & Anderson, E. F. (2020). Streamlining Photogrammetry Reconstructions of Bone Fragments for Bioarchaeological Analysis, Conservation, and Public Engagement. *Eurographics 2020 - Posters*, 2 pages. https://doi.org/10.2312/EGP.20201036

Redman, S. J. (2016). *Bone Rooms: From Scientific Racism to Human Prehistory in Museums*. Harvard University Press.

Remondino, F. (2011). Heritage Recording and 3D Modeling with Photogrammetry and 3D Scanning. *Remote Sensing*, *3*(6), Article 6. https://doi.org/10.3390/rs3061104

Rogers, T., & Saunders, S. (1994). Accuracy of Sex Determination Using Morphological Traits of the Human Pelvis. *Journal of Forensic Sciences*, *39*(4), 1047–1056. https://doi.org/10.1520/JFS13683J

Schug, G. R., Killgrove, K., Atkin, A., & Baron, K. (2020). 3D Dead: Ethical Considerations in Digital Human Osteology. *Bioarchaeology International*, *4*(3–4), Article 3–4. https://doi.org/10.5744/bi.2020.3008

Schutkowski, H. (1993). Sex determination of infant and juvenile skeletons: I. Morphognostic features. *American Journal of Physical Anthropology*, *90*(2), 199–205. https://doi.org/10.1002/ajpa.1330900206

Shearer, B. M., Sholts, S. B., Garvin, H. M., & Wärmländer, S. K. T. S. (2012). Sexual dimorphism in human browridge volume measured from 3D models of dry crania: A new digital morphometrics approach. *Forensic Science International*, *222*(1), 400.e1-400.e5. https://doi.org/10.1016/j.forsciint.2012.06.013

Souri, S. (1959). *A morphological study of the fetal pelvis*. *8*, 45–55.

Spradley, M. K., & Jantz, R. L. (2011). Sex Estimation in Forensic Anthropology: Skull Versus Postcranial Elements. *Journal of Forensic Sciences*, *56*(2), 289–296. https://doi.org/10.1111/j.1556-4029.2010.01635.x

Steyn, M., & İşcan, M. Y. (2008). Metric sex determination from the pelvis in modern Greeks. *Forensic Science International*, *179*(1), 86.e1-86.e6. https://doi.org/10.1016/j.forsciint.2008.04.022

The Foundry Visionmongers Limited. (2020). *Mari*. https://www.foundry.com/products/mari

Thomas, D. H. (2000). *Exploring Native North America* (1st edition). Oxford University Press.

Thomson, A. (1899). The Sexual Differences of the Fœtal Pelvis. *Journal of Anatomy and Physiology*, *33*(Pt 3), 359-526.5.

Ubelaker, D. H. (2011). United States of America. In N. Marquez-Grant & L. Fibiger (Eds.), *The Routledge Handbook of Archaeological Human Remains and Legislation: An international guide to laws and practice in the excavation and treatment of archaeological human remains* (pp. 533–540). Routledge.

Ulguim. (2017). Recording In Situ Human Remains in Three Dimensions. *Human Remains: Another Dimension*, 71–92.

Ulguim. (2018). Models and Metadata: The Ethics of Sharing Bioarchaeological 3D Models Online. *Archaeologies*, *14*(2), 189–228. https://doi.org/10.1007/s11759-018-9346-x

Umbach, D., & Jones, K. N. (2003). A few methods for fitting circles to data. *IEEE Transactions on Instrumentation and Measurement*, *52*(6), 1881–1885. https://doi.org/10.1109/TIM.2003.820472

Valenzuela, G. de L., & Julia, M. (2014). *Three-dimensional image technology in forensic anthropology: Assessing the validity of biological profiles derived from CT-3D images of the skeleton*. https://open.bu.edu/handle/2144/15358

Vandenbossche, V., Valcke, M., Willaert, W., & Audenaert, E. (2022). From bones to bytes: Do manipulable 3D models have added value in osteology education compared to static images? *Medical Education*, *n/a*(n/a). https://doi.org/10.1111/medu.14993

Ventola, C. L. (2014). Medical Applications for 3D Printing: Current and Projected Uses. *Pharmacy and Therapeutics*, *39*(10), 704–711.

Verhoff, M. A., Ramsthaler, F., Krähahn, J., Deml, U., Gille, R. J., Grabherr, S., Thali, M. J., & Kreutz, K. (2008). Digital forensic osteology—Possibilities in cooperation with the Virtopsy® project. *Forensic Science International*, *174*(2), 152–156. https://doi.org/10.1016/j.forsciint.2007.03.017

Wachowiak, M., & Karas, B. (2009). 3d Scanning and Replication for Museum and Cultural Heritage Applications. *Journal of the American Institute for Conservation*, *48*, 141–158. https://doi.org/10.1179/019713609804516992

Walker, P. L. (2005). Greater sciatic notch morphology: Sex, age, and population differences. *American Journal of Physical Anthropology*, *127*(4), 385–391. https://doi.org/10.1002/ajpa.10422

Walker, P. L. (2008). Sexing skulls using discriminant function analysis of visually assessed traits. *American Journal of Physical Anthropology*, *136*(1), 39–50. https://doi.org/10.1002/ajpa.20776

Weber, G. W., & Bookstein, F. L. (2011). *Virtual Anthropology: A guide to a new interdisciplinary field*. Springer-Verlag. https://www.springer.com/gp/book/9783211486474

White, T. D., Black, M. T., & Folkens, P. A. (2012). *Human Osteology* (3rd edition). Academic Press.

Wild, S. (2020, January 10). *3D Printing and the Murky Ethics of Replicating Bones*. Undark Magazine. https://undark.org/2020/01/10/3d-bone-prints-south-africa/

Winchester, J. M. (2016). MorphoTester: An Open Source Application for Morphological Topographic Analysis. *PLOS ONE*, *11*(2), e0147649. https://doi.org/10.1371/journal.pone.0147649

Wrobel, G. D., Biggs, J. A., & Hair, A. L. (2019). Digital Modeling for Bioarchaeologists. *Advances in Archaeological Practice*, *7*(1), 47–54. https://doi.org/10.1017/aap.2018.47

CURRICULUM VITAE